Journal of the Indian Institute of Science
A Multidisciplinary Reviews Journal
ISSN: 0970-4140 Coden-JIISAD

REVIEWS

Weyl Semi-Metals: A Short Review

Sumathi Rao

Abstract | We begin this review with an introduction and a discussion of Weyl fermions as emergent particles in condensed matter systems, and explain how high energy phenomena like the chiral anomaly can be seen in low energy experiments. We then explain the current interest in the field due to the recent discovery of real materials which behave like Weyl semi-metals. We then describe a simple lattice model of a topological insulator, which can be turned into a Weyl semi-metal on breaking either time-reversal or inversion symmetry, and show how flat bands or Fermi arcs develop. Finally, we describe some new phenomena which occur due to the chiral nature of the Weyl nodes and end with possible future prospects in the field, both in theory and experiment.

1 Introduction

In recent times, the Landau paradigm of classification of states through the principle of spontaneous symmetry breaking and local order parameters has been superseded by classification through topology or global properties of the many-body ground state wave-function of the system.[1] These topological phases have some property to which an integer can be assigned, which is robust and depends only on global properties. They cannot be destroyed by local perturbations such as disorder and scattering, as long as the bulk gap is not closed, although they can have surface metallic states—in fact, surface metallic states are what distinguishes them from ordinary insulating phases.

The first, most famous example of a topological phase is the integer quantum Hall effect.[2] This was a system of electrons moving in two dimensions, with a strong perpendicular magnetic field (time-reversal broken system). This led to Landau levels and most importantly, to the quantisation of the transverse conductance with remarkable accuracy. It was soon realised that this effect had a topological explanation[3]–the physically measured transverse current was related to a topological invariant, the first Chern number, which is just the integral of the Berry curvature over the Brillouin zone. The topological phase on each plateau was protected by a bulk gap, and the current was carried by metallic surface or edge states.

However, for a long time, this did not have much impact on material science, because quantum Hall effect occurred at low temperatures and at very high magnetic fields. There was a lattice model proposed by Haldane[4] which suggested that materials could have topologically nontrivial band structures, characterised by non-zero Chern numbers, even without an external magnetic field. But it is only in the last decade or so that it was realised that this could occur in realistic materials. Consequently, there has been an explosion of work on topological materials.[5] The hallmark of these materials was that they were insulating in the bulk, but they could conduct electricity through metallic surface states, without magnetic field or breaking time-reversal invariance. Hence, unlike the quantum Hall phases, these materials had to have a pair of counter-propagating edge states due to time-reversal invariance. Also, unlike the quantum Hall phases, they could occur in three dimensions as well as in planar systems. Furthermore, in these systems, the edge or surface states had relativistic dispersions and hence, the physics of Dirac fermions became relevant in these materials.

But more recently, it has been realised that gaplessness is not an essential ingredient for topological protection. Band topology can be defined, even if the gap closes at some points in the Brillouin zone. A particular example of such a phase is the Weyl semi-metal phase,[6] which was

Integer quantum Hall effect: This is a quantum mechanical version of the Hall effect, where a voltage is induced perpendicular to the direction of motion, when two dimensional electrons are subjected to a strong magnetic field. The conductance in the direction perpendicular to the applied voltage is found to be quantised in units of e^2/h and this is called the integer quantum Hall effect.

Harish-Chandra Research Institute, Chhatnag Road, Jhusi, Allahabad India.
sumathi@hri.res.in

first predicted in the pyrochlore iridates.[7] It is a new state of matter, whose low energy excitations are Weyl fermions. Unlike the topological insulators, these materials have gapless states in the bulk as well as the boundary.

2 Emergent Weyl Fermions in Condensed Matter Systems

Dirac and Weyl fermions: In 3+1 dimensions, the standard spin 1/2 fermion which describes quarks and leptons are Dirac fermions. In general, they have a mass, have relativistic dispersions and are described by 4 component spinors which obey the Dirac equation. But when the mass is turned off, the Dirac equation splits into two Weyl equations, whose solutions in terms of two component spinors describe Weyl fermions. These are two massless particles that transform differently under the Poincare group and have their spins oppositely aligned to their directions of motion.

Chirality and helicity: Chirality essentially means asymmetry with respect to mirror reflection. In particle physics, massless fermions can either be left-handed or right-handed depending on how their wave-function transforms under the Poincare group. Helicity, on the other hand, is the sign of the projection of the spin along the direction of motion, which in principle can be changed, except for massless particles, where it becomes an attribute of the particle and is the same as the chirality.

The idea that particles with relativistic dispersion can be quasiparticles in condensed matter systems is not new and goes back to the early days of the study of Luttinger liquids,[8] where it was realised that close to the Fermi energy, the dispersion could be linearised and obeyed relativistic energy-momentum relations.

More recently, relativistic Dirac fermions came into prominence with the discovery of graphene[9] in 2+1 dimensions. Graphene is a single sheet of carbon atoms arranged in a honeycomb lattice. Electrons moving around the carbon atoms interact with the periodic potential of the honeycomb lattice to give rise to a Fermi surface with six double cones where the valence and conductance bands touch each other. (Out of these six, only two are independent). Close to these nodes, the dispersion is linear and the Hamiltonian is given by the massless relativistic Dirac equation, with the speed of light replaced by the Fermi velocity and the spin replaced by the pseudo-spin of the sub-lattices —

$$H = v_F(\sigma_x p_x + \sigma_y p_y). \tag{1}$$

The wave-functions are two component spinors with the spinor index refering to the sublattice index and real spin being an additional quantum number. v_F is the Fermi velocity in the solid, which replaces the speed of light in relativistic systems. The low energy excitations about the nodes are gapless (graphene is metallic). However, in principle, they can be gapped out by perturbations (mass terms) proportional to σ_z. The stability of graphene comes from the extra symmetries under time-reversal and spatial inversion,[10] which enforces the vanishing of terms proportional to σ_z and hence implies that no gap is induced, as long as perturbations do not break time-reversal and inversion symmetry.

A possible generalisation of this to 3+1 dimensions is to write down the massless 3+1 Dirac Hamiltonian given by

$$H = \begin{pmatrix} 0 & v_F\vec{\sigma}\cdot\mathbf{p} \\ v_F\vec{\sigma}\cdot\mathbf{p} & 0 \end{pmatrix} \tag{2}$$

This is equivalent to having two doubly degenerate Dirac cones at the same point in momentum space. This is what has been dubbed as a Dirac semi-metal.[11] This semi-metal can also be gapped out easily by adding mass terms proportional to a diagonal 4×4 matrix ($I_{2\times2}$, $-I_{2\times2}$). However, the Dirac points can be protected by crystal symmetries, and provided that the perturbations or imperfections that exist do not break this symmetry, semi-metallic phases can be observed.

However, it is possible to split the degeneracy of the Dirac node in momentum space or energy space by breaking either time-reversal or inversion symmetry. This gives rise to two Weyl nodes with opposite chiralities (or helicities), whose dispersion is given by the massless Weyl Hamiltonian. The basic idea[6] behind the existence and stability of these Weyl nodes is very simple. Close to the degeneracy points where two non-degenerate bands touch each other and the energy is cone-like, the electronic excitations are described by the Weyl equation, simply because the effective Hamiltonian at that point has to have two dimensions, and besides the identity, there are only three anti-commuting σ matrices. More explicitly, the low energy Hamiltonian for a two band model is given by

$$H = a(\mathbf{k}) + \sigma\cdot\mathbf{b}(\mathbf{k}), \tag{3}$$

where $\sigma = (\sigma_x, \sigma_y, \sigma_z)$ are the three Pauli matrices. We can now expand the Hamiltonian around the touching or gapless points ($\mathbf{k} = \mathbf{k}_0$) in the Brillouin zone to get

$$H(\mathbf{k}\simeq\mathbf{k}_0) \simeq \text{const} + \sigma\cdot\mathbf{b}(\mathbf{k}_0) + \sigma\cdot\frac{\partial b_i}{\partial k_j}_{(\mathbf{k}=\mathbf{k}_0)}(\mathbf{k}-\mathbf{k}_0). \tag{4}$$

This is precisely the Weyl Hamiltonian (though offset and anisotropic) and the wave-functions are two component Weyl fermions with positive or negative chirality. These band-touching points or nodes can move around in the momentum space, by perturbations that change the Hamiltonian slightly, but the only way for them to gap out and disappear is if they meet another node with the opposite chirality. This is very different from what happens in graphene. In fact, a straighforward generalisation of the graphene Hamiltonian to 3+1 dimensions can also be made simply by adding a term proportional to σ_z to obtain

$$H = \sigma_x p_x + \sigma_y p_y + \sigma_z p_z, \tag{5}$$

which is just the isotropic form of the model given in Eq. 4 and is the familiar Weyl Hamiltonian in relativistic systems. Here, there is no fourth anti-commuting matrix to add a mass term.

Perturbations can only move the nodes, but cannot gap them out. Hence, we have gapless fermions with a single chirality at each band touching point.

Surprisingly, it was found, initially through detailed calculations,[7,12,13] that there are condensed matter materials, whose band structure shows nodes or points around which the excitations are Weyl fermions. These materials were dubbed Weyl semi-metals (WSM).[14] They also have very unusual surface states called Fermi arcs, which terminate at the location of the bulk Weyl nodes, which we will discuss in detail later.

As was already mentioned, in a system with both inversion symmetry and time-reversal symmetry intact, one always gets Dirac nodes — both left and right handed chiral nodes, at the same point, in which case it is always possible to add a mass term using the fourth anti-commuting four component γ matrix and gap it out. So to get Weyl nodes in the condensed matter system, one needs to break either inversion symmetry or time-reversal symmetry.

The stability of the Weyl nodes can also be connected to a topological quantum number, which is the conservation of the total charge of the Weyl nodes. As we said above, a single Weyl node cannot disappear by itself. It has to annihilate with a Weyl node of the opposite charge. This also means that for the Weyl nodes to have well-defined coordinates, momentum has to be a good quantum number, so translational invariance has to be unbroken. So disorder has to be fairly weak.

Also, Weyl nodes can be thought of as monopoles in momentum space. The charge of the Weyl node can be related to the quantised Berry flux, which can be computed from the momentum space wave-functions of the filled states near the Weyl node. It turns out to be $\pm 2\pi\kappa$ depending on the chirality of the node (positive or negative) and the 'monopole' charge κ.[6] The topological stability of the Weyl node is thus related to the Gauss law, which keeps the total flux inside a given surface invariant. The Weyl node can only vanish when it annihilates with another Weyl node with opposite chirality. Also, since the net charge of all the Weyl nodes inside a Brilloiuin zone has to be zero, the Weyl nodes always come in pairs and the minimum number of Weyl nodes that one can have in any model is two.[15]

3 The 'High Energy' Connection

The distance between high energy physics and condensed matter physics has been decreasing in recent years, with the so-called (AdS-CFT) Anti-de Sitter- Conformal Field theory (or even AdS-CMT for condensed matter theory) connection.[16] But in the field of Dirac materials, the connection is much more direct and the idea that quasiparticles can be relativistic fermions is quite old.[8] Moreover, with the discovery of topological materials, there has been a possibility of seeing even Majorana modes (not exactly Majorana fermions, but related) and now Weyl fermions in low energy condensed matter settings. We will discuss the discovery of these Weyl fermions in the next section, but in this section, we will see how phenomena such as the chiral anomaly related to Weyl fermions get translated in the condensed matter context.

Majorana fermions and Majorana modes: In particle physics, Majorana fermions are fundamental particles whose creation operator is the same as its annihilation operator. They are real fermions, as opposed to complex Dirac fermions. In the condensed matter context, they are hermitean operators satisfying the anti-commutation relations. However, they are not real fermions and obey non-abelian statistics under exchange.

The basic idea of the chiral anomaly is that the conservation laws $\partial_\mu j^\mu = 0$ and $\partial_\mu j_5^\mu = 0$ cannot be simultaneously satisifed. So if we take the conservation of current to be sacrosanct, the current of the left and right chirality fermions cannot be individually conserved. The Adler-Bell-Jackiw anomaly equation[17]

$$\partial_\mu j_5^\mu = FF^*/8\pi^2 \tag{6}$$

thus leads to breaking of the chiral symmetry by the anomaly. In the Weyl semi-metal context, these equations can be rewritten as

$$\frac{\partial}{\partial t}(n_R + n_L) = 0, \Rightarrow \frac{\partial}{\partial t}(n_R - n_L) \neq 0,$$
$$\frac{\partial}{\partial t}(n_R - n_L) = \pm\frac{e^2}{h^2}\mathbf{E}\cdot\mathbf{B}, \tag{7}$$

where n_R and n_L denote the number of fermions at the right and left chirality Weyl nodes. This implies that by applying parallel electric and magnetic fields, we can change the difference in their numbers, or if we have really have an isolated Weyl node, we can change the number of particles. This is essentially a quantum mechanical effect because the path integral for Weyl fermions coupled to an electromagnetic field is not invariant under independent gauge transformations of the left and right chiral fields. So single chirality fermions implies charge non-conservation. However, in any real system, one always has total particle number conservation. Hence, Weyl nodes in any crystal always have to come in pairs. Due to the anomaly term, we can get charge pumping between the nodes—n_R decreases and n_L increases or vice-versa, at a rate given by the anomaly. But the total number of particles remains the same. This is called the Nielsen-Ninomiya theorem.[15]

More formally, by coupling the Weyl fermions to an external electromagnetic field and computing

the effective action by integrating out the fermions, it can be shown that the time-reversal or parity breaking parameter in the model leads to an effective θ term in the action given by

$$S_\theta = \frac{e^2}{32\pi^2}\int d^4x\theta(x)\varepsilon^{\mu\nu\alpha\beta}F_{\mu\nu}F_{\alpha\beta}, \quad (8)$$

(we are using 4 vector notation here and μ runs from 0 to 3) where the axion field $\theta(x) = 2b_\mu x^\mu = 2\mathbf{b}\cdot\mathbf{r} - 2b_0 t$ and $b_\mu = b_0$, b_i are parameters that break the parity (b_0) and time-reversal (b_i). The current can be computed from the effective action and is found to be

$$j^\nu = \frac{e^2}{2\pi^2}b_\mu\varepsilon^{\mu\nu\alpha\beta}\partial_\alpha A_\beta, \quad \mu = 1,2,3$$
$$\text{and} \quad j^\nu = \frac{e^2}{2\pi^2}b_0\varepsilon^{0\nu\alpha\beta}\partial_\alpha A_\beta . \quad (9)$$

The first equation above describes the anomalous Hall effect, with the Hall conductance proportional to the separation between the Weyl nodes

$$\sigma_{xy} = e^2/h \times |\mathbf{b}|. \quad (10)$$

The second equation describes the chiral magnetic effect, which naively seems to imply equilibrium currents in the presence of a magnetic field.[18,19] But the notion of the chiral anomaly in a condensed matter system is itself somewhat idealised, because unlike in the relativistic case where chiral symmetric is exact for massless fermions, here, even the relativistic dispersion for the Weyl fermions and chiral symmetry is only approximately true, close to the Weyl nodes. Hence, using the chiral anomaly directly to predict effects in the Weyl semi-metal is not a very good idea. More detailed calculations have shown that the first result can be rederived in different ways,[20] but the second result involving the naive expectation of equilibrium currents is incorrect in the condensed matter context.[21] As pointed out in Ref. 22, in a Weyl semi-metal, although there is a charge imbalance at the nodes due to the anomaly, there is also a return path for the charges via the Fermi arcs on the surfaces. Hence, one needs to be careful in applying relativistic ideas directly to the Weyl semi-metal system.

So the basic idea to look for effects of the anomaly, would be to apply parallel electric and magnetic fields to the system and see whether there are explicit effects due to the charge imbalance between the two chiral nodes in the condensed matter system itself. One would expect the results to be highly anisotropic, because the effect depends on the angle between the applied electric field and the magnetic field, being maximum when $\mathbf{E} \parallel \mathbf{B}$ and minimum (vanishing) when $\mathbf{E} \perp \mathbf{B}$. In fact, there have been several works[23,24] that have explicitly computed the physical effects of the chiral anomaly in Weyl semi-metals. They have shown that the chiral anomaly actually leads to large negative longitudinal magneto-resistance at weak fields, as expected from the anomaly equation. More recently, there has been work[25] that has shown that the chiral anomaly generically leads to longitudinal magneto-resistance (LMR) in three dimensional chiral metals (not necessarily Weyl semi-metals and not necessarily even Dirac materials). In a Weyl semi-metal, the sign of the LMR depends on the kind impurities in the sample, and generically, with both ionic and neutral impurities, the LMR becomes negative initially and then becomes positive as a function of the magnetic field.

Other effects of the anomaly such as current induced by strain fields[19], anisotropic non-local voltage drops[26] and optical absorption[27] due to the charge imbalance between the two nodes have also been studied. For inversion symmetry breaking semi-metals, the chiral nodes are at two different energies, which leads to a chiral chemical potential between the nodes. This can give rise to measurable optical signals.[28] Other effects include unusual plasmon modes[29] in doped WSM. All these possibilities have spurred experimental activity in this field and in the last few months, there has been definite evidence for Weyl fermions in several materials.

4 Current Excitement due to 'Discovery' of Weyl Fermions

The initial proposals for Weyl semi-metals included pyrochlore iridates,[7] $HgCr_2Se_4$[13] and topological insulator-normal insulator heterostructures,[12] but there is no experimental evidence for them yet. Negative magnetoresistance was observed experimentally[30] when magnetic field was applied to *BiSb* tuned to its critical point (the Dirac point) between normal and topological insulator, but that by itself was not convincing enough to confirm the existence of Weyl fermions, particularly since it was realised that negative magneto-resistance is generic in three dimensional metals. However, in the last few months, there has been a lot of excitement[31] in the field, ever since the publication of direct evidence for not only the Weyl nodes, but also the Fermi arcs in the non-centrosymmetric material *TaAs* using ARPES (angle resolved photoemission spectroscopy) techniques, by the Princeton group[32] and a group from the Chinese Academy of Sciences.[33] They were able to show co-propagating Fermi arcs

Time reversal symmetry: Time reversal symmetry implies a system which looks the same when you reverse the sign of time. In quantum mechanics, it is represented as an anti-unitary symmetry. For particles with 1/2 integer spin, this leads to the Kramer's theorem which states that all time-reversal invariant states are doubly degenerate.

Parity symmetry: Parity symmetry implies a system which looks the same when you reverse the signs of all the spatial coordinates. It is distinct from symmetry under rotation. For instance, in two spatial dimensions, parity is defined as inversion of only one of the coordinates, because inverting both of them would be equivalent to a rotation.

terminating at the Weyl nodes with non-zero chiral charges of ±2. At the same time, Weyl nodes were also seen in a photonic crystal, which was 'made to order' to reproduce a desired band structure.[34] Both these cases involved inversion symmetry breaking. In *TaAs*, the crystal structure itself lacked inversion symmetry and in the photonic crystal, inversion symmetry breaking was explicitly incorporated. The photonic crystal was made such that it realises 4 Weyl nodes (the minimum for inversion symmetry breaking Weyl semi-metals), whereas *TaAS* has 24 Weyl nodes. Fermi arcs have also been observed in Dirac semi-metals, such as Cd_3As_2[35] and Na_3Bi.[36] Other candidate materials include an inversion symmetry breaking stochiometric compound $SrSi_2$[37] that forms a WSM without spin-orbit coupling and an exotic state with quadratic dispersion when spin-orbit coupling, is included, but this has not yet been confirmed. For a recent review of topological semi-metals predicted from first principle calculations, see.[38]

5 Explicit Lattice Model and Phase Diagram

We will now study some features of the WSM in detail,[39] using a simple tight-binding four-band lattice model[21,40] for the topological insulator (TI) in three dimensions (3DTI), whose phases can describe strong and weak topological insulators, Weyl semi-metals and ordinary insulators depending on the values of the various parameters of the model. Many 3DTI materials, including the family belonging to the Bi_2Se_3 class, have an effective description in terms of the Hamiltonian given by $H_0 = H_C + H_{SO}$[21] with

$$H_C = \varepsilon \sum_j \psi_j^\dagger \tau_x \psi_j - t \sum_{\langle ij \rangle} \psi_i^\dagger \tau_x \psi_j + \text{h.c.}$$

$$\text{and} \quad H_{SO} = i\lambda_{SO} \sum_j \psi_j^\dagger \tau_z \left(\sigma_x \psi_{j+\hat{y}} - \sigma_y \psi_{j+\hat{x}} \right) + i\lambda_z \sum_j \psi_j^\dagger \tau_y \psi_{j+\hat{z}} + \text{h.c.} \tag{11}$$

Here z is the direction of growth of the crystal, and σ and τ denote Pauli matrices in spin and orbital (parity) space respectively. ε and t denote the standard on-site and nearest neighbour hopping amplitudes. λ_{SO} and λ_z are the (possibly anisotropic) spin-orbit (SO) interaction strengths in the x-y plane and in the z direction respectively. i, j refer to site indices in all three dimensions. The topological invariants for the 3DTI, $\nu_\mu = (\nu_0; \nu_1, \nu_2, \nu_3$ can be easily obtained using parity invariance[41] and are given by[39]

$$(-1)^{\nu_0} = \text{sgn}\left[(\varepsilon - 6t)(\varepsilon + 6t)(\varepsilon - 2t)^3(\varepsilon + 2t)^3\right],$$
$$(-1)^{\nu_i} = \text{sgn}\left[(\varepsilon + 6t)(\varepsilon - 2t)(\varepsilon + 2t)^2\right],$$

for $i = 1, 2, 3$. Depending on the values of the invariants, we have the following phases:

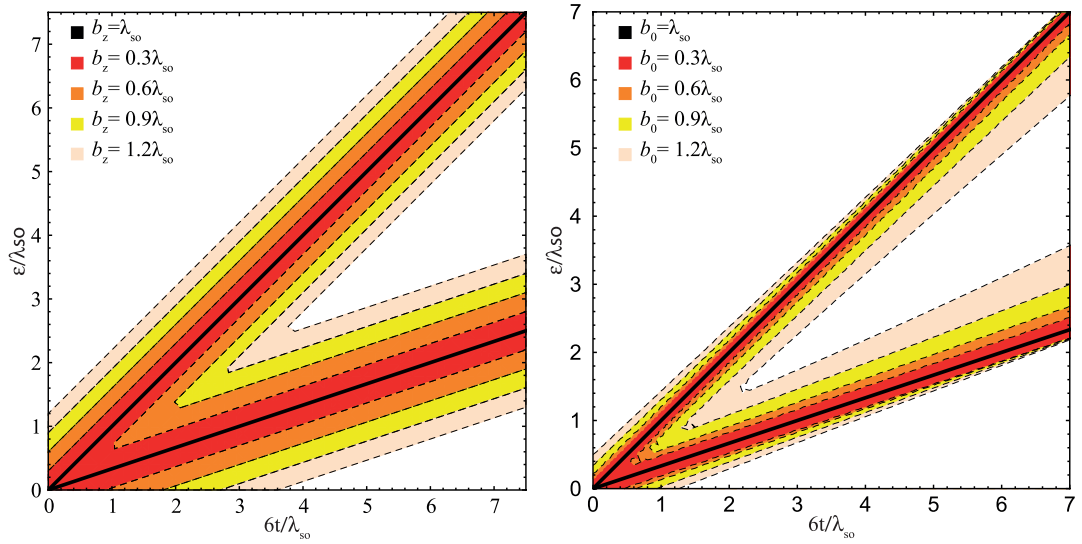

Figure 1: (Color online) Typical phase diagrams of our model system. The Weyl semi-metal (WSM) phase appears at the strong topological insulator (STI)/normal insulator (NI) ($\varepsilon = 6t$) and strong topological insulator (STI)/weak topological insulator (WTI) ($\varepsilon = 2t$) boundaries (shown by black lines) with broken time reversal (b_z)/parity (b_0) perturbations. The WSM phase extends with increasing perturbations in the filled regions. Parameters used here are $\lambda_z = \lambda_{SO}$.

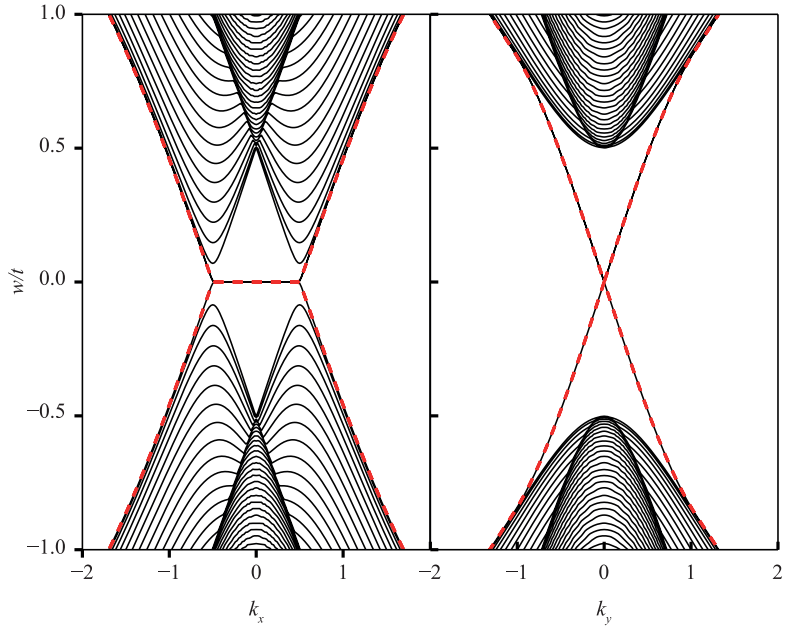

Figure 2: (Color online) The dispersion for a WSM with 2 Weyl nodes at $k_0 = \pm b_x/\lambda_z$ is shown along k_x and k_y. The parameters used are **b** = (0.50*t*, 0, 0), $\lambda_{SO} = \lambda_z = 0.50t$. The dashed (red) lines denote the surface band.

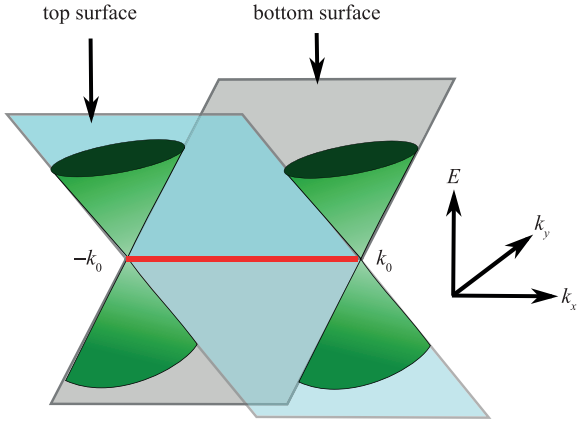

Figure 3: (Color online) The dispersion for a WSM with 2 Weyl nodes at $\pm k_0$. The blue and grey surfaces show the dispersions of the surface states on the top and bottom surfaces respectively. The cones represent the bulk states and the picture shows how the surface states merge into the bulk.

$$\begin{array}{lll} |\varepsilon| > |6t| & \nu_\mu = (0;0,0,0) & \text{Ordinary Insulator} \\ |6t| > |\varepsilon| > |2t| & \nu_0 = 1 & \text{Strong Topological Insulator (STI)} \\ |2t| > |\varepsilon| > 0 & \nu_0 = (0;1,1,1) & \text{Weak Topological Insulator (WTI)} \end{array} \quad (12)$$

The Weyl semi-metal (WSM) phases arise close to the boundaries of the topological phase transitions, at $\varepsilon \approx \pm 6t, \pm 2t$ when either parity (inversion) or time reversal (TR) symmetry or both are broken. In other words, the Hamiltonian for the WSM is given by $H_W = H_0 + H_E$ where

$$H_E = \sum_j \psi_j^\dagger \left(b_0 \tau_y \sigma_z - b_x \tau_x \sigma_x + b_y \tau_x \sigma_y + b_z \sigma_z \right) \psi_j \,. \quad (13)$$

Here b_0 and **b** are parameters that break inversion and TR symmetry respectively and

separate the Dirac point of the TI into two Weyl points, with the separation being in energy and in momentum space respectively.[21] An arbitrary Hermitean term can be added to this Hamiltonian, whose effect will be to cause the Weyl nodes to move around. However, for small perturbations, it cannot remove the nodes. The nodes can only vanish if the perturbation is large enough to bring both the Weyl nodes together. The phase diagram of the different phases in this model is given in Fig. 1.[39]

The band structure of the WSM is given in Fig. 2.[39] As can be seen from there, the cones that describe the Fermi surface around each of the nodes are independent for small enough doping (small values of the chemical potential or Fermi energy E_F). But for larger values of the chemical potential, they merge into a single Fermi surface. For sufficiently large system size, the dispersion is flat between the two Weyl nodes along the k_x direction, and is linear along k_y (for k_x values between the Weyl nodes). These are the surface states (in momentum space) and are shown in Figs. 2 and 3.

6 Characteristics of Surface States and Fermi Arcs

The existence of surface states for TI is well-established. They are isolated from the bulk states, since the bulk is gapped, and they are spin-momentum locked–i.e., the spin is tied to the direction of motion, and opposite spins travel in opposite directions. This has been explicitly seen in many experiments[42] using scanning tunneling microscopy. Surface states also exist for the WSM. This is more unexpected because one does not expect well-separated surface states in a gapless model, since they are expected to merge with the bulk states. So the first question that one has to answer is why surface states exist at all. It is because the system (to a good approximation) is translationally invariant. Hence, momentum is a good quantum number and it is possible to have surface states at momenta where there are no bulk states–ie., between the Weyl nodes.

It is also found that the surface states at the Fermi energy in WSM form an arc and not a full Fermi surface. These Fermi arcs end at the projection of the Weyl nodes onto the surface, where the surface mode is no longer well-defined, because it merges into the bulk modes. What does this mean? An intuitive picture[14] to understand Fermi arcs is to start with a very thin sample of Weyl semi-metal and slowly increase the thickness so that the two surfaces are pulled apart. To start with, we have a complete Fermi surface, but as the thickness increases, complementary parts of the Fermi surface get attached to the two surfaces and they get connected to one another through the Weyl nodes in the bulk. A picture of how the surface states at the two opposite surfaces with opposite chiralities get connected through the bulk states is given in Fig. 3. This is essentially the same dispersion that is shown in Fig. 2 separately along the k_x axis and k_y axis.

We now study the surface states for both the TI and WSM phases in the specific four band (finite-size) model that we have studied in the previous section where TR is broken. For strong topological insulators, surface states exist on each surface as mid-gap states[5] in the band structure, whereas in weak topological insulators, surface states arise only on particular surfaces depending on the values of ν_i (i = 1, 2, 3).[43] For Weyl semi-metals, in our model, inversion symmetry breaking does not give rise to surface states. Surface states arise only when TR is broken at the phase boundary between the normal and the topological insulator. For instance, if we choose the TR symmetry to be broken by $\mathbf{b} = b_x \hat{x}$, then each Dirac point yields a pair of Weyl nodes with a separation of $b_x / \lambda_z \hat{x}$ in momentum space, and we note that away from the Weyl nodes, there is a gap in the spectrum. If we put the chemical potential at the energy of the Weyl nodes, we can consider the state obtained by filling all the negative energy states. By studying how this state evolves as a function of the crystal momentum, we define the Berry phase and the Berry flux $\mathcal{B}(k) = \nabla_k \times \mathcal{A}(k)$. The Weyl nodes here are the sources of this flux $\nabla \mathcal{B}(k) = \pm \delta^3 (k - k_\pm)$.

Since the Weyl nodes can be thought of as sources and sinks of Berry phase monopoles, there is a flux penetrating all the two-dimensional layers between the nodes. All these layers have non-zero Chern number, whereas two-dimensional planes not between the nodes have zero Chern number. So the two-dimensional planes between the nodes are like quantum Hall planes, and they all exhibit integer quantum Hall effect and have edge states. In other words, for each value of k_x between the Weyl nodes, we have a Chern insulator. This is precisely the reason that there is an anomalous Hall effect as shown in Eq. 10 proportional to the separation between the Weyl nodes. The Fermi arc is just the line that one gets by stringing the edge states of the Chern insulator together and clearly these states only exist between the Weyl nodes. This is illustrated in Fig. 4. It also clear from the figure that surface states can only exist on the x-y and x-z planes. No surface states exist on the y-z planes since the separation between the Weyl nodes is along the x-axis.

Now, let us look at the surface states of this model in detail. The first surprise is that there are

Berry phase and Berry curvature: The Berry phase or geometric phase or Pancharatnam-Berry phase is the phase acquired over a closed cycle when the parameters of a system are slowly (adiabatically) changed and brought back to themselves. This can be non-trivial if the space spanned is not simply connected. The Berry phase can be expressed in terms of a connection or Berry potential and the anti-symmetric second-rank tensor derived from it is called the Berry curvature.

Magnetic monopoles: A magnetic monopole is a hypothetical particle with a magnetic charge violating $\vec{\nabla} \cdot \mathrm{B} = 0$. In the condensed matter context, they are quasi-particles and not sources of real magnetic field, but only some effective magnetic field. In that sense, they only resemble magnetic monopoles.

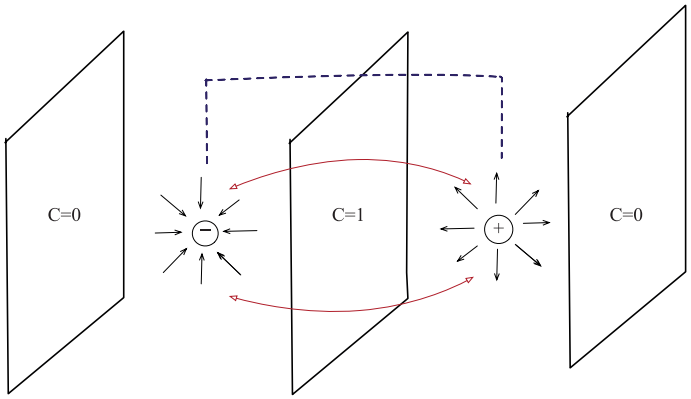

Figure 4: (Color online) The Berry phase monopoles of charge ±1 at the two Weyl nodes of opposite chirality. The two dimensional planes within the nodes are quantum Hall planes with non-zero Berry flux passing through it and hence non-zero Chern number. The Fermi arcs are the edge states of the quantum Hall planes strung together.

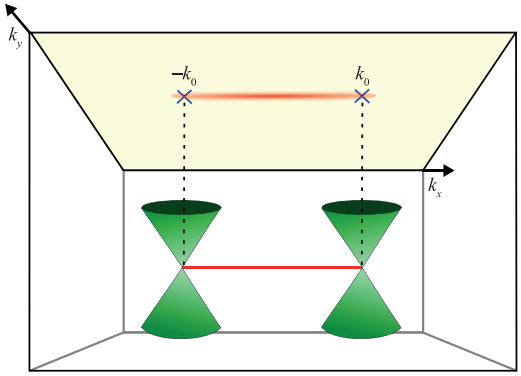

Figure 5: (Color online) The local (surface) density of states (LDOS) for a WSM with 2 Weyl nodes at $\pm k_0$. The red line shows finite value for LDOS, whereas the yellow region denotes zero LDOS. Note that surface states appear on the ***x-y*** and ***x-z*** planes, but not along the ***y-z*** planes.

surface states, because there is no gap. So, if we put the chemical potential at the position of the Weyl nodes, there are not only gapless surface states, but also gapless bulk states at the same chemical potential at the nodes. So we may think that the surface states should hybridise with the bulk states. But as we mentioned earlier, momentum conservation implies that it is possible to have surface states at momenta where there are no bulk states – ie., between the Weyl nodes. So at these values of the momentum, we will only have surface states and no bulk states, the material will appear like a topological insulator. When we look at the the local density of states of the real position-space surface of the three dimensional WSM as a function of the momentum, at the Fermi energy (tuned to the Weyl nodes), we find that they form an arc, (in this particular model, it forms a straight line) between the momenta k_0 and $-k_0$, the positions of the Weyl nodes, instead of a closed curve. This is shown in Fig. 5. At the Weyl nodes, there is no distinction between the surface states and bulk states, and they merge into the bulk. But between the Weyl nodes, the surface states are well-defined. As discussed above, the surface states are essentially the edge states of the quantum Hall planes strung together.

There has also been a detailed study[44] of the evolution of the surface states (Fermi arcs) to form a single Dirac cone as the parameters of a time-reversal (TR) symmetric, but inversion symmetry broken WSM are changed to become a TI.

As we mentioned earlier, the excitement in this field has increased many-fold[31] since the actual visualisation of the Fermi arcs by the Princeton and Chinese Academy of Sciences groups.[32,33]

7 New phenomena in Weyl semi-metals

Weyl semi-metals have bulk conducting states, and hence, are metallic. However, there are many ways

in which their behaviour is different from the usual metals. The metallic states exist only for some values of momenta and at other values of momenta, there is a gap to excitations. The excitations at the nodes are chiral, and hence their spin is aligned to the direction of motion. All of this leads to new transport phenomenon, which exists only for Weyl semi-metals. In this section, we will discuss some new results that occur when Weyl semi-metals are placed in proximity with superconductors.

Motivated by the fact that the introduction of superconductivity via either proximity effect or by introducing a pairing Δ term in the bulk leads to a new topological phase in the topological insulator, we studied[39] what happens when a Weyl semi-metal is tunnel coupled to an *s*-wave superconductor. We started with the model described in Sec. (4) with two Weyl nodes separated by the time-reversal breaking parameter **b** in the *x*-direction. We took the model to be infinite in the *y* direction, so that k_y is a good quantum number and we took *z* to be finite, so that the surface states existed at the top and bottom in the *z*-direction. We coupled one of the surfaces of the WSM to an *S*-wave superconductor and then integrated out the superconducting degrees of freedom to obtain an effective action for the WSM. We then obtained the local density of states (LDOS) and the induced pairing in the WSM using a Green's function technique as well as exact diagonalisation. We found that the flat band due to the Fermi arc states split into two when proximity coupled to the WSM, each carrying half the Chern number of the original surface state, but it does not gap out fully. The gap remains at the Weyl nodes. This is seen in Fig. 6,[39] and can be understood as follows. The *S*-wave superconducting correlations couples the electrons at one node of a certain chirality to holes at the other node, but of the same chirality (because the two nodes have opposite chirality, but electrons and holes also have opposite chirality). Hence, no gap can open up, because a mass term requires fermions of opposite chirality.

We have also studied[45] the reflection and Andreev reflection (the phenomenon where an electron incident on a superconductor bounces back as a hole and two electrons (a Cooper pair) goes into the superconductor) that takes place at the junction between a Weyl semi-metal and a superconductor. A scattering approach[46] showed that the differential conductance depended on the

Andreev reflection: This is a process by which an electron gets reflected as a hole at the interface between a normal metal and a superconductor and a charge 2e is transferred into the superconductor as a Cooper pair. This happens below the superconducting gap, because there is no possibility for single particle transmission into the superconductor.

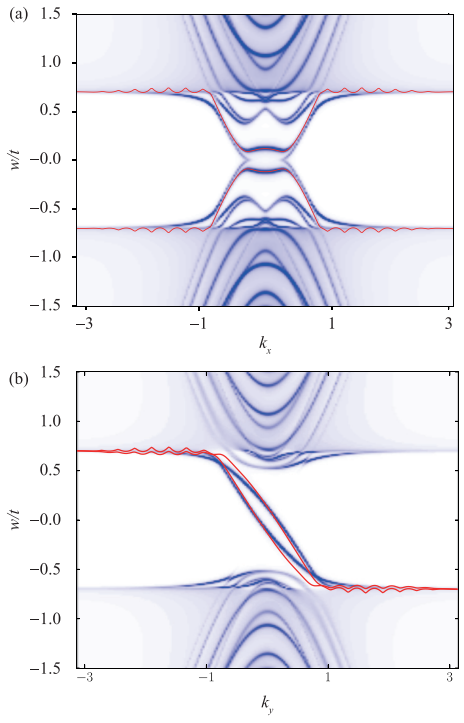

Figure 6: (Color online) The effect of the proximity induced superconductivity in the surface bands of the WSM with momenta (a) k_x and (b) k_y where the Weyl nodes lie along k_x. The blue (gray) high density lines are the modified bands in the system with proximity to the superconductor obtained from the LDOS at $z = 0$ using a Green's function technique, while the red (darker) solid line is the surface band at $z = 0$ via exact diagonalization. The induced gap vanishes at the Weyl nodes for a large enough system size, but the surface band splits. Various parameters used for the LDOS are $\lambda_{SO} = \lambda_z = 0.5t$, $\Delta = 0.7t$, $\lambda_S = 0.9t$, $\varepsilon = 6t$, **b** = (0.5*t*, 0, 0) and number of sites in *z* is 20. We have used $k_y = 0$ for (a) and $k_x = 0$ for (b).

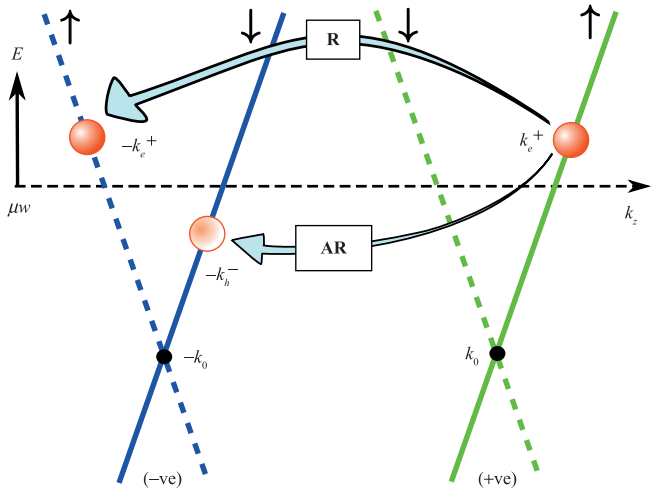

Figure 7: (Color online) Both reflection (R) and Andreev reflection (AR) in a WSM occur from one chiral node to another. The chiralities of the nodes are denoted as +ve and −ve, whereas the solid and the dashed lines show dispersions of the fermions at the two Weyl nodes with positive and negative velocities (=dE/dk). The spins of the bands (denoted by arrows) and the need to conserve spin accounts for the change of chirality for both normal and Andreev reflection.

angle between the current and the vector connecting the two Weyl points. For the simplest model of a time-reversal breaking Weyl semimetal with two nodes, we showed that both normal and Andreev reflection change chirality—see Fig. 7.[45] We also showed that the existence of a new momentum scale introduced by the time-reversal leads to the non-vanishing of normal reflection, unlike in graphene, where at low energies close to Fermi energy, the current is purely due to Andreev reflection and normal reflection vanishes.

We also showed that when the Weyl semi-metal is sandwiched between two superconductors, the Josephson current shows unexpected oscillations as a function of the time-reversal breaking parameter as shown in Fig. 8. For normal metals, the current is expected to be independent of the length L for short ballistic Josephson junctions. For graphene, which is a Dirac metal, it was shown that the critical current has diffusion-like scaling proportional to $1/L$ at the Dirac point, but without any impurity scattering.[47] But for the Weyl semi-metal, apart from the 2π periodicity in φ (which is the phase difference between the two superconductors), we also find a periodicity in the length L with period π/k_0. This is shown in Fig. 8.[45] Moreover, we also find the zero-pi transition[48] of the Josephson current characteristic of superconductor-ferromagnet-superconductor junctions, which is perhaps not surprising, since the WSM that we studied violated time-reversal invariance. Here the Josephson current was computed for the lattice model of the WSM studied in Sec. (5) through its Green's function, $g(\omega) = [(\omega + i\delta)\mathcal{I} - H_0]^{-1}$, which was coupled to two superconductors on either side of it, through an onsite self-energy[39]

$$\Sigma_i(\omega) = \frac{\tilde{t}}{\sqrt{\Delta^2 - \omega^2}}(\mathcal{I}_\tau + \tau^x)[\omega\mathcal{I}_\zeta - \Delta e^{i\varphi_i}\zeta^x]\mathcal{I}_\sigma. \tag{14}$$

Here ζ acted on the particle-hole degree of freedom of the model defined in the Nambu basis and Σ_i was defined only on the sites in contact with the i^{th} superconductor. Δ denoted the S-wave pair potential in the superconductor. Then writing the full Green's function as $G(\omega) = (g^{-1}(\omega) - \Sigma_L(\omega) - \Sigma_R(\omega))^{-1}$, we computed the Josephson current.[45]

Josephson current: Josephson current is the current that flows across a device called the Josephson junction which is made of two superconductors with a phase difference ϕ separated by an insulator, metal or just a tunneling junction.

8 Future Challenges and Opportunities

The experimental discovery of Weyl semi-metals may lead to new and unexpected spintronic applications. Weyl fermions are gapless and hence have high mobility and can travel with very little resistance.They have topological protection because once a Weyl node is formed, it can only annihilate if there is another Weyl node of opposite chirality and they are brought together. They are also chiral and their spin is aligned to the direction of motion.

In the next few years, there is considerable scope in the experimental front for discovering new candidate materials for Weyl semi-metals, particularly with time-reversal symmetry breaking, which has not yet been seen. On the theoretical front, massless Weyl fermions had been studied

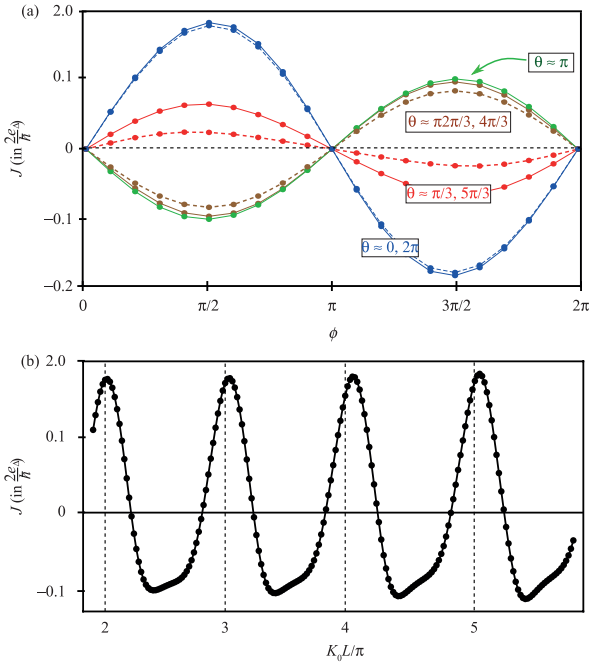

Figure 8: (Color online) (a) Josephson current as a function of the superconducting phase difference ϕ for various values of $\theta = 2k_0L$ mod(2π) and (b) Josephson current as a function of the length (k_0L/π) at $\phi = \pi/2$. The parameters used are $\tilde{t} = 0.25t$, $\varepsilon = 6t$, $\lambda = \lambda_z = t$, $\Delta = 0.01t$, $\mu = 0.02t$ and $L = 60$ sites. For these parameters, the position of Weyl nodes, $k_0 \approx k_z$.

for many years in high energy physics as a possible candidate of neutrinos, before the mass for neutrinos was discovered. It would be of interest to see whether any of the more exotic effects like neutrino oscillations have possible manifestations in the condensed matter context. The study and classification of gapless topological materials is also far from complete and will also probably gain centre-stage in the next few years.

Acknowledgments

I would like to thank my collaborators Udit Khanna, Arijit Kundu and Dibyakanti Mukherjee for many useful discussions on many aspects of topological insulators and Weyl semi-metals.

Received 7 March 2016.

References

1. A.P. Schnyder *et al.*, Phys. Rev. B **78**, 195125 (2008); A. Kitaev, AIP Conf. Proc. **1134** (2009); X.L. Qi *et al.*, Phys. Rev. B **78**, 195424 (2008).
2. R. Prange and S.M. Girvin, The Quantum Hall effect, Springer (1990); For more recent reviews, see, for instance, M.O. Goerbig, Les Houches summer school lecture notes, cond-mat/0909.1998; O. Heinonen, 'Composite fermions: A unified view of the quantum Hall regime', World Scientific, Singapore (1998), etc.
3. D.J. Thouless *et al.*, Phys. Rev. Lett. **49**, 405 (1982).
4. F.D.M. Haldane, Phys. Rev. Lett. **61**, 2015 (1988).
5. C.L. Kane and E.J. Mele, Phys. Rev. Lett. **95**, 226801 (2005); ibid, Phys. Rev. Lett. **95**, 146802 (2005); C. Wu, B.A. Bernevig, and S.C. Zhang, Phys. Rev. Lett. **96**, 106401 (2006); B.A. Bernevig, T.L. Hughes, and S.C. Zhang, Science **314**, 1757 (2006); J.E. Moore and L. Balents, Phys. Rev. B **75**, 121306 (2007); R. Roy, Phys. Rev. B. **79**, 195321 (2009); M. König, H. Buhmann, L.W. Molenkamp, T.L. Hughes, C.-X. Liu, X.L. Qi, and S.C. Zhang, J. Phys. Soc. Jpn. **77**, 031007(2008); M. König, S. Wiedmann, C. Brune, A. Roth, H. Buhmann, L. Molenkamp, X.-L. Qi, and S.-C. Zhang, Science **318**, 766 (2007). For reviews, see M.Z. Hassan and C.L. Kane, Rev. Mod. Phys. **82**, 3045 (2010); X.L. Qi and S.C. Zhang, Rev. Mod. Phys. **83** , 1057 (2011); M.Z. Hassan and J.E. Moore, Ann. Rev. Cond. Matt. Phys. **2**, 55 (2011); Y. Ando, J. Phys. Soc., Jpn **82**, 102001 (2013).
6. S. Murakami, New J. Phys. **9**, 356 (2007).
7. X. Wan, A.M. Turner, A. Vishwanath and S.Y. Savrasov, Phys. Rev. B **83**, 205101 (2011); P. Hosur, S.A. Parameswaran and A. Vishwanath, Phys. Rev. Lett. **108**, 046602 (2012).
8. For reviews, see for instance, A.O. Gogolin, A.E. Nersesyan and A.M. Tsvelik, Bosonisation and Strongly Correlated systems, Cambridge University Press, 1998; T. Giamarchi, Quantum Physics in One dimension, Oxford Science publications 2004.
9. See for instance, A.H. Castro Neto *et al.*, Rev. Mod. Phys. **81**, 109 (2009).
10. J.L. Manes *et al.*, Phys. Rev. **B 75**, 155424 (2007).
11. Z. Wang *et al.*, Phys. Rev. B **85**, 195320 (2012); Z. Wang *et al.*, Phys. Rev. **B 88**, 125427 (2013).

12. A.A. Burkov and L. Balents, Phys. Rev. Lett. **107**, 127205 (2011); A.A. Burkov, M.D. Hook and L. Balents, Phys. Rev. B **84**, 235126 (2011).
13. G. Xu *et al.*, Phys. Rev. Lett. **107**, 186806 (2011).
14. For reviews, see for instance, A.M. Turner and A. Vishwanath, cond-mat/1301.0330; P. Hosur and X. Qi, cond-mat/1309.4464, Comptes Rendus Physique, **14**, 857 (2013).
15. H.B. Nielsen and M. Ninomiya, Phys. Lett. **B105**, 219 (1981).
16. S. Sachdev, Scientific American, **308**, 44 (2013)
17. S. Adler, Phys. Rev. **177**, 2426 (1969); J.S. Bell and R. Jackiw, Nuovo Cimento A **60**, 47 (1969).
18. A.A. Zyusin and A.A. Burkov, Phys. Rev. B **86**, 115133 (2012); D.T. Son and N. Yamamoto, Phys. Rev. Lett. **109**, 181602 (2012); Y. Chen *et al.*, Phys. Rev. B **88**, 125105 (2013); P. Goswami and S. Tewari, Phys. Rev. B **88**, 245107 (2013); A.G. Grushin, Phys. Rev. D **86**, 045001 (2012).
19 J. Zhou *et al.*, Chin. Phys. Lett. **30**, 027101 (2013).
20. K. Yang *et al.*, Phys. Rev. B **84**, 075129 (2011).
21. M.M. Vazifeh and M. Franz, Phys. Rev. Lett. **111**, 027201 (2013).
22. See talk by Haldane at WPI-MANA International workshop, NIMS, Tsukuba, Japan, April 2014, online at http://wwwphy.princeton.edu/ haldane/research.html.
23. A.A. Burkov, Phys. Rev. Lett. **113**, 247203 (2014); A.A. Burkov, Phys. Rev. B **91**, 245157 (2015).
24. E.V. Gorbar, V.A. Miransky and I.A. Shovkovy, Phys. Rev. B **89**, 085126 (2014).
25. P. Goswami *et al.*, Phys. Rev. B **92**, 075205 (2015).
26. S.A. Parameswaran *et al.*, Phys. Rev. **X4**, 031035 (2014).
27. P.E.C. Ashby and J.P. Carbotte, Phys. Rev. B **89**, 245121 (2014).
28. P. Goswami, G. Sharma and S. Tewari, Phys. Rev. B **92**, 161110 (2015).
29. J. Zhou *et al.*, Phys. Rev. B **91**, 035114 (2015).
30. H.J. Kim *et al.*, Phys. Rev. Lett. **111**, 246603 (2013).
31. See for example, A.A. Zyuzin *et al.*, Phys. Rev. B **85**, 165110 (2012); V. Aji, Phys. Rev. B **85**, 241101 (2012); T. Ojanen, Phys. Rev. B **87**, 245112 (2013); T. Das, Phys. Rev. B **88**, 035444 (2013); Z. Huang *et al.*, New Joul of Phys. **15**, 123019 (2013); P.E.C. Ashby and J.P. Carbotte, Eur. J. Phys. B, **87** (2014); J. Maciekjo and R. Nandkishore, Phys. Rev. B **90**, 035126; S. Ganeshan and S. Das Sarma, Phys. Rev. B **91**, 125438 (2015); E.V. Gorbar *et al.*, Phys. Rev. B **90**, 115131 (2014); Y.X. Zhao and Z.D. Wang, Phys. Rev. Lett. **114**, 206602 (2015); A. Altland and D. Bagrets, Phys. Rev. Lett. **114** 257201 (2015); J. Behrends *et al.*, Phys. Rev. B **93**, 075114 (2016); A.A. Soluyanov *et al.*, Nature **527**, 495 (2015); J. Klier, I.V. Gornyi and A.D. Mirlin, Phys. Rev. B **92**, 205113 (2015); Y. Baum *et al.*, Phys. Rev. **X5**, 041046 (2015); A. Altland and D. Bagrets, Phys. Rev. B **93**, 075113 (2016); S. Kourtis *et al.*, Phys. Rev. B **93**, 041109 (2016); S. Bera, J.D. Sau and B. Roy, archive preprint, cond-mat/1507.07551; C.K. Chan *et al.*, archive preprint, cond-mat/1509.05400; P. Baireuther *et al.*, archive preprint, cond-mat/1512.02144; Y. Zhang *et al.*, archive preprint, cond-mat/1512.06133; A.A. Zyusin and R.P. Tiwari, archive preprint, cond-mat/1601.00890; A. Chen and M. Franz, archive preprint, cond-mat/1601.01727.
32. S.Y. Xu *et al.*, Science **349**, 613 (2015).
33. B.Q. Lv *et al.*, Phys. Rev. **X5**, 031013 (2015).
34. L. Lu *et al.*, Science **349**, 622 (2015).
35. M. Neupane *et al.*, Nature Comm. **5**, 10.1038/ncomms4786 (2014); Z.K. Liu *et al.*, Nature Mat. **13**, 677 (2014).
36. Z.K. Liu *et al.*, Science **343**, 864 (2014).
37. S.M. Huang *et al.*, Archive preprint, cond-mat/1503.05868.
38. H. Weng *et al.*, archive preprint, cond-mat/1603.04744.
39. U. Khanna, A. Kundu, S. Pradhan and S. Rao, Phys. Rev. B **90**, 195430 (2014).
40. P. Delplace, J. Li and D. Carpentier, Europhys. Lett. **97**, 67004 (2012).
41. L. Fu and C.L. Kane, Phys. Rev. Lett. **100**, 096407 (2008).
42. H.T. Hsieh *et al.*, Nature **452**, 970 (2008); Y. Xia *et al.*, Nat. Phys. **5**, 398 (2009).
43. L. Fu and C.L. Kane, Phys. Rev. B **76**, 045302 (2007).
44. R. Okugawa and S. Murakami, Phys. Rev. B **89**, 235303 (2013).
45. U. Khanna, D.K. Mukherjee, A. Kundu and S. Rao, cond-mat/1509.03166, accepted for publication in Phys. Rev. B (RC).
46. S. Uchida, T. Habe, and Y. Asano, J. Phys. Soc. Jpn. **83**, 064711 (2014).
47. M. Titov and C.W.J. Beenakker, Phys. Rev. B **74**, 041401(R), 2006.
48. L.N. Bulaevski *et al.*, JETP Lett. **25**, 290 (1977); A.I. Buzdin *et al.*, JETP Lett. **35**, 178 (1982); For reviews, see A.A. Golubov *et al.*, Rev. Mod. Phys. **76**, 411 (2004); A.I. Buzdin, Rev. Mod. Phys. **77**, 935 (2005).

Sumathi Rao got her PhD from the State University of New York (USA) in 1983 in the field of particle physics after doing her Master's at the Indian Institute of Technology in Mumbai. She returned to the Institute of Physics in Bhubaneswar in 1987 with a faculty position after her post-doctoral stints at Fermilab and University of Wisconsin at Madison in the US. She is currently a Professor at the Harish-chandra Research Institute in Allahabad, where she has been since 1995, and where she and her students have been working, in recent times, in the area of transport in mesoscopic and low-dimensional systems, which is a sub-field of condensed matter physics.

Sumathi Rao has made seminal research contributions in both high energy physics and condensed matter physics. She has mentored several students who are now faculty members in different institutes in India. She has been elected as a fellow of the National Academy of Science in 2001. She was also one of the initiators of the International Union of Pure and Applied Physics (IUPAP) international conferences of women in physics and has been an important part of the world-wide movement to improve the representation of women in physics.